geoconvention
Calgary • Canada • May 15-19 2017

Alternating first-arrival traveltime tomography and waveform inversion for near-surface imaging

Mengyao Sun, Jie Zhang and Wei Zhang

School of Earth and Space Sciences, University of Science and Technology of China

Summary

Near-surface seismic imaging often plays a significant role in producing quality data processing results for the deep subsurface in land and shallow marine environments. First-arrival traveltime tomography is a common approach for near-surface imaging due to its high efficiency and simplicity. However, the method faces issues of missing hidden layers or low-velocity anomalies and resolving the structures with low resolution. On the other hand, waveform inversion should offer better solutions for dealing with these issues but may suffer from the cycle skipping problem. We intend to use the advantages and reduce the disadvantages of the two methods by developing a new strategy of alternately applying traveltime tomography and waveform inversion through iterations. First-arrival traveltime tomography applies a wavefront raytracer and a nonlinear inversion approach. Waveform inversion is a multiscale approach in which the wavelet is applied in the data domain to better handle the cycle skipping problem. By alternating the two inversions rather than performing a joint inversion, we reduce the memory requirements and avoid non-physical scaling problems between the two approaches. Using a synthetic example, we demonstrate that alternating inversions minimize two separate objective functions at the same time and constrain the near surface structures fairly well.

Introduction

Solving near-surface statics problem is often critial in land or shallow marine seismic data processing. First-arrival traveltime tomography (Zhang and Toksöz, 1998; Zhu et al., 2008) is a standard approach for imaging the near-surface velocity structures due to its efficiency and simplicity. However, traveltime tomography may fail to reveal low velocity anomalies and hidden layers and may also fail to resolve detailed structures with high resolution. Full-waveform inversion (FWI) has been developed to address these problems (Tarantola, 1988). However, the objective function of FWI includes numerous local minima.In the data domain, the problem is well known as cycle skipping if the predicted data from a starting model differs from the acquired data by half a period(Shin and Cha, 2009; Fei et al., 2012; Baeten et al., 2013; Chi et al., 2014). For getting over the cycle skipping problem, a lot of methods has been tried. Such as multiscale waveform inversion method (Bunks et al., 1995), which gradually inverts from low-wavenumber to high-wavenumber structures. The precondition of the multiscale method is that the global solution on one scale is always in the convex neighborhood of the global minimum of the next smaller scale. However, it cannot be theoretically guaranteed valid for all applications. The joint inversion method is considered another way to solve the local minima problem (Zhang et al., 2014). While, there is a non-physical scaling factor between different inversion-problems, which is very essential to the final result. Therefore, we intend to use the advantages and reduce the disadvantages of these methods by developing a new strategy of alternately applying traveltime tomography and waveform inversion through iterations, which will involve both traveltime and waveform information during the inversion and avoid dealing with the scaling factor problem.

Theory

The alternate inverison is performed by applying waveform inversion and traveltime tomography alternately. The first-arrrival traveltime tomography applies a wavefront raytracer and a nonlinear inversion approach. Waveform inversion is a multiscale approach in which the wavelet transform is applied in

data domain to better handle the cycle skipping problem.

The initial model $\mathbf{m}_{ini}$ of the alternate inversion is built by the common method of first-arrival traveltime tomography. The multiscale waveform inversion is then first performed on the large-scale data we set. The result obtianed by the waveform inversion is the initial model and the structural constraint of the traveltime tomography. The procedures should then be repeated in the next iteration and for the next smaller scale. The workflow of the alternate inversion is shown in the pseudocode (see Algorithm 1), where, $scale$ is the current scale for the inversion, $iter$ is the current iteration of the inversion, $itermax$ is the maximum iteration number that we set, $scale_{start}$ and $scale_{end}$ are the start scale and the final scale, respectively, $\mathbf{m}_{fwi}$ is the inversion result of the multiscale waveform inversion at this stage, $\mathbf{m}_{tt}$ is the first-arrival traveltime tomography result at this stage. $s(\mathbf{x}_r, \mathbf{x}_s, t; \mathbf{m})$ represents the synthetic waveforms, $d(\mathbf{x}_r, \mathbf{x}_s, t)$ is the observed waveforms. $\mathbf{x}_r$ and $\mathbf{x}_s$ are the positions of the receivers and shots, respectively. $\mathbf{m}$ is the model slowness. t is the time window for the inversion. $\mathbf{L}$ is the Laplacian operator for model regularization and α is a constant parameter for balancing the data misfit and the model regularization. $\mathbf{d}_{obs}$ is the observed traveltime data and $G(\mathbf{m})$ contains the calculated traveltimes. λ has the same meaning as α. Finally, the output is $\mathbf{m}_{tt}$ or $\mathbf{m}_{fwi}$, because they are almost the same in the end of the entire inversion procedure.

Algorithm 1: Alternate inversion

Input : Observed data $d_{scale}(\mathbf{x}_r, \mathbf{x}_s, t)$ and $\mathbf{d}_{obs}$, initial model $\mathbf{m}_{ini}$
Output: $\mathbf{m}_{tt}$ or $\mathbf{m}_{fwi}$
Initialize: $iter = 1$; $scale = scale_{start}$;
while $scale <= scale_{end}$ **do**
  while $iter <= itermax$ **do**
    $\Phi_{scale}(\mathbf{m}_{fwi}) = \sum_{s,r} \int (s_{scale}(\mathbf{x}_r, \mathbf{x}_s, t; \mathbf{m}_{ini}) - d_{scale}(\mathbf{x}_r, \mathbf{x}_s, t))^2 dt + \alpha ||\mathbf{L}(\mathbf{m}_{fwi})||^2$
    $\Psi(\mathbf{m}_{tt}) = ||\mathbf{d}_{obs} - G(\mathbf{m}_{tt})||^2 + \lambda ||\mathbf{L}(\mathbf{m}_{tt} - \mathbf{m}_{fwi})||^2$
    $\mathbf{m}_{ini} = \mathbf{m}_{tt}$
    $iter = iter + 1$
  end
  $scale = scale + 1$
end

Synthetic test

We implement the alternate inversion on a synthetic test. In the following we will use the result obtained by the waveform inversion method alone as the comparison to evaluate the improvements of the new method. Figure 1a shows the true model of the synthetic test, which includes two layers imbeded in a background with a constant gradient. The model measures $5000\ m \times 600\ m$ and the grid size is $10\ m \times 10\ m$. The sketch of the acquisition geometry is shown in Figure 1b. We use red and yellow dots to represent the shots and receivers, respectively. The survey geometry includes 80 shots and 160 receivers for every shot with a $60\ m$ shot spacing and $30\ m$ receiver interval, respectively. After obtaining the simulated true data, we decompose the waveforms into eight levels and reconstruct them from scale 5 down to scale 4 and scale 0 formally captures all original signals.

Figure 1b shows the initial model for the two differente inversion methods, which is built by first-arrival traveltime tomography. First, we perform the wavelet-based multiscale waveform inversion without involving the traveltime information. The inversion results of different scales are displayed in Figures 1c, 1d and 1e. Figure 1e is the final result. We then perform the alternate inverseion using the same initial model. Figures 1f, 1g and 1h display the inversion reuslts obtained by the alternate inversion method, and Figure 1h is the final result.

In the results obtained by the two different methods, we observe that when the data scale turns

from large to small, the structures are inverted gradually and the resolution becomes higher. For the waveform inversion method alone, we notice that although it can roughly invert the two layers, the shapes are distorted, and more artifacts are present in the results. However, the result obtained by the alternate inversion reveals the two layers for the better positions, the velocity values, and the structure shapes. Additionally, a more reliable background velocity is presented after finishing the last scale inversion.

We show the waveform overlay and the traveltime overlay of the final results, which are obtained by the two different methods (Figure 2). Both waveforms and traveltimes show better fitting performance for the alternate inversion method compared with the waveform inversion method alone. Furthermore, a notable cycle skipping phenomenon occurs in Figure 2a. However, it converges to the global minimum for the alternate inversion method by involving both waveform and traveltime information and avoids droping into the local minima.

Conclusions

We propose a new inversion method by combining both wavelet-based multiscale waveform and traveltime inversions through iterations. The synthetic test verifies that this method can reduce the chance of dropping into the local minima. Compared with the wavelet-based multiscale waveform inversion alone, the alternate inversion method can maintain both the traveltime and waveform fitting at the same time. We also observe that this method can suppress the cycle skipping phenomenon to some degree in practical applications.

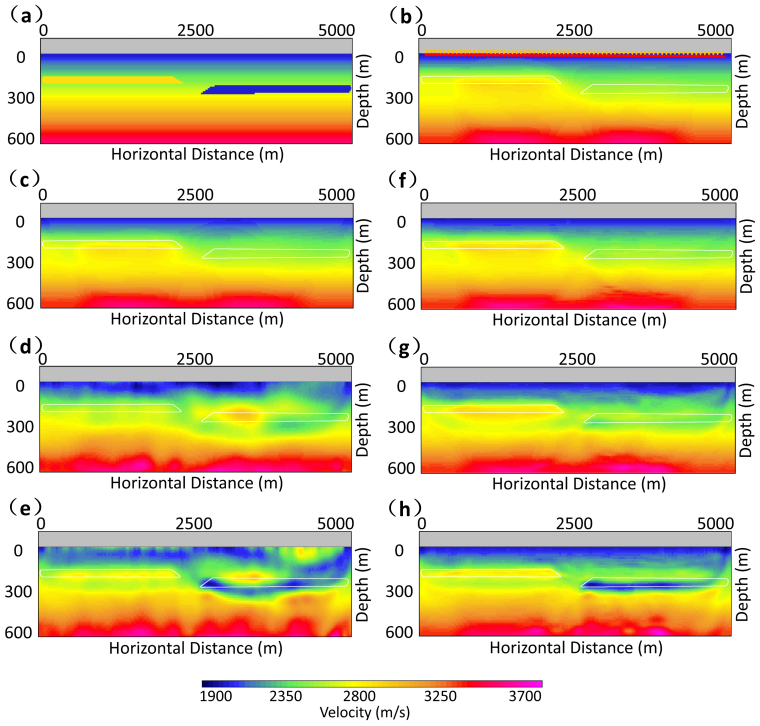

Figure 1: A synthetic test and comparison. The inversion results obtained by the two different methods. The white lines mark the true positions of the layers. (a) The true model. (b) The initial model built by the first-arrival traveltime tomography. (c), (d) and (e) are the results of scale 5, scale 4 and scale 0 which are obtained by performing the waveform inversion method alone. (f), (g) and (h) are the results of applying the alternate inversion method associated with scale 5, scale 4 and scale 0 data representations.

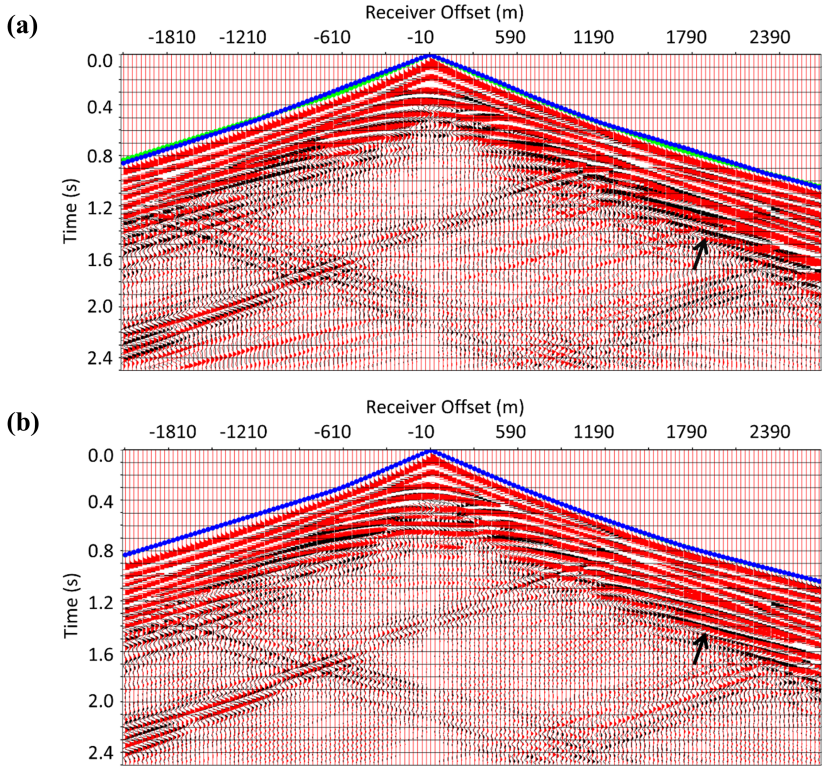

Figure 2: The waveform and traveltime overlay of the synthetic test. The black waveforms are the simulated true data. The red waveforms are the synthetics of the final inversion results. The green dots are the simulated true traveltimes and the blue ones are the synthetics of the final inversion results. (a) The overlay display of the waveform inversion method alone. The black arrows point out the waveforms where the cycle skipping occurs. (b) The overlay display of the alternate inversion method.

Acknowledgements

We gratefully acknowledge the financial support of the National Natrual Science Foundation of China (Grant No. 41374132). We also appreciate GeoTomo for allowing us to use the TomoPlus software package.

References

Baeten, G., J. W. de Maag, R.-E. Plessix, R. Klaassen, T. Qureshi, M. Kleemeyer, F. t. Kroode, and Z. Rujie, 2013, The use of low frequencies in a full-waveform inversion and impedance inversion land seismic case study: Geophysical Prospecting, **61**, 701–711.

Bunks, C., F. M. Saleck, S. Zaleski, and G. Chavent, 1995, Multiscale seismic waveform inversion: Geophysics, **60**, 1457–1473.

Chi, B., L. Dong, and Y. Liu, 2014, Full waveform inversion method using envelope objective function without low frequency data: Journal of Applied Geophysics, **109**, 36–46.

Fei, T. W., Y. Luo, F. Qin, P. G. Kelamis, et al., 2012, Full waveform inversion without low frequencies: A synthetic study: Presented at the 2012 SEG Annual Meeting, Society of Exploration Geophysicists.

Shin, C., and Y. H. Cha, 2009, Waveform inversion in the laplacefourier domain: Geophysical Journal International, **177**, 1067–1079.

Tarantola, A., 1988, Theoretical background for the inversion of seismic waveforms including elasticity and attenuation: Pure and Applied Geophysics, **128**, 365–399.

Zhang, J., J. Chen, et al., 2014, Joint seismic traveltime and waveform inversion for near surface imaging: Presented at the 2014 SEG Annual Meeting, Society of Exploration Geophysicists.

Zhang, J., and M. N. Toksöz, 1998, Nonlinear refraction traveltime tomography: Geophysics, **63**, 1726–1737.

Zhu, X., P. Valasek, B. Roy, S. Shaw, J. Howell, S. Whitney, N. D. Whitmore, and P. Anno, 2008, Recent applications of turning-ray tomography: Geophysics, **73**, VE243–VE254.